Available online at www.sciencedirect.com
ScienceDirect
International Journal of Plasticity 24 (2008) 1581–1605
INTERNATIONAL JOURNAL OF Plasticity
www.elsevier.com/locate/ijplas

A multi-length scale sensitivity analysis for the control of texture-dependent properties in deformation processing

Veera Sundararaghavan [a], Nicholas Zabaras [b,*]

[a] *Department of Aerospace Engineering, University of Michigan, Ann Arbor, MI 48109, USA*
[b] *Materials Process Design and Control Laboratory, Sibley School of Mechanical and Aerospace Engineering, Cornell University, Ithaca, NY 14853, USA*

Received 20 July 2007; received in final revised form 10 December 2007
Available online 25 December 2007

Abstract

Material property evolution during processing is governed by the evolution of the underlying microstructure. We present an efficient technique for tailoring texture development and thus, optimizing properties in forming processes involving polycrystalline materials. The deformation process simulator allows simulation of texture formation using a continuum representation of the orientation distribution function. An efficient multi-scale sensitivity analysis technique is then introduced that allows computation of the sensitivity of microstructure field variables such as slip resistances and texture with respect to perturbations in macro-scale forming parameters such as forging rates, die shapes and preform shapes. These sensitivities are used within a gradient-based optimization framework for computational design of material property distribution during metal forming processes. Effectiveness of the developed computational scheme is demonstrated through computationally intensive examples that address control of properties such as Young's modulus, strength and magnetic hysteresis loss in finished products.

Keywords: Multi-scale modelling; Continuum sensitivity analysis; Polycrystal plasticity; Materials-by-design; Forming process design

* Corresponding author. Tel.: +1 607 255 9104; fax: +1 607 255 1222.
E-mail address: zabaras@cornell.edu (N. Zabaras).
URL: http://mpdc.mae.cornell.edu/ (N. Zabaras).

0749-6419/$ - see front matter © 2007 Elsevier Ltd. All rights reserved.
doi:10.1016/j.ijplas.2007.12.005

1. Introduction

Realization of optimal material properties is important to address the critical performance needs of hardware components in aerospace, naval and automotive applications. Newly emerging property design strategies for metallic materials are aimed towards tailoring microstructural subsystems by controlling processes that govern their evolution (Olson, 1997). An example is in composite design, where techniques that enable tailoring of microstructure topology have allowed identification of structures with interesting extremal properties such as negative thermal expansion (Sigmund and Torquato, 1996) and negative Poisson's ratio (Lakes, 2000). One such technique for optimizing properties of metallic materials, comprised of a polycrystalline microstructure, involves tailoring of preferred orientation of crystals manifested as the crystallographic texture. During forging and extrusion processes, mechanisms such as crystallographic slip and lattice rotation drive formation of texture and variability in property distributions in polycrystalline materials. A possible method for designing property distribution in such materials is to control the deformation so that textures with desired properties are obtained. Several applications exist where certain textures are desirable to improve properties of materials. For example, a Goss texture is desirable in transformer cores to reduce power losses during magnetization (Rollett et al., 2001). In deep drawing, a high value of texture-dependent R parameter (Hosford, 1993) and low planar anisotropy is necessary to prevent earing and to increase drawability of the sheet.

Recent developments in microstructure-sensitive design have addressed problems such as computing optimal textures that lead to desired properties from the space of all possible textures (Adams et al., 2001; Kalidindi et al., 2004). The problem of identification of processing paths that lead to such optimal textures is being addressed using novel means such as representation of processing paths in microstructure spaces using spectral (Li et al., 2005) or reduced order representations (Sundararaghavan and Zabaras, 2007) and using gradient optimization techniques (Acharjee and Zabaras, 2003; Sundararaghavan and Zabaras, 2006). However, the success of such process design techniques has only been demonstrated at the microstructural length scale. The novelty in this work is that process design is performed using two different length scales. The macro-scale is associated with the component being modelled (10^{-3}–10^{1} m) and the meso-scale is characterized by the underlying polycrystalline microstructure (10^{-6}–10^{-3} m). We address the design problem of computation of macro-scale parameters such as forging velocity, die and preform shapes such that microstructure evolution is tailored towards achieving desired properties.

The optimization problem involves minimizing an objective function that is an error measure between the desired property and the numerically calculated properties for a given set of macro-scale parameters. A sensitivity analysis scheme is used for calculating the gradient of the objective function and to drive the optimization procedure (Srikanth and Zabaras, 2001; Zabaras et al., 2003). Posed in a multi-scale sense, the approach is used to compute sensitivities of microstructural fields such as slip resistance, crystal orientations due to perturbations in macro-scale parameters. These sensitivities are exactly defined using a set of field equations developed by directly differentiating the governing equations with respect to small perturbations in the macro-scale process parameters. An averaging principle is then developed to compute sensitivity of stress and various material properties at the macroscopic level from microstructural sensitivity fields. Evolution of the micro-scale during forming is modelled using continuum representation of texture (Kumar

and Dawson, 1996, 1997; Ganapathysubramanian and Zabaras, 2005) and incorporates crystal elasto-plasticity through the constitutive equations of Anand and Kothari (1996). Effectiveness of the developed computational scheme is demonstrated through examples involving control of properties such as Young's modulus, strength and magnetic hysteresis loss in finished products.

The paper is arranged as follows. In Section 2, the direct deformation model is briefly defined. This includes details about the microstructure representation, the constitutive model for polycrystalline materials and the kinematic problem in the context of a multi-length scale analysis. Section 3 develops the multi-length scale kinematic sensitivity problem. Section 4 considers a set of examples to demonstrate the accuracy, performance and applicability of the proposed algorithms.

2. Direct deformation problem

To supplement the continuum sensitivity model developed in the next section and to introduce our notation, we first briefly present the direct deformation model used in our analysis. In this work, polycrystalline microstructure at each material point in the macro-continuum is represented using an underlying orientation distribution function (ODF) (Bunge, 1983; Kocks et al., 2000). The ODF $\mathscr{A}$ is represented over the Rodrigues–Frank (RF) fundamental region following our work in Ganapathysubramanian and Zabaras (2005). When texture development is modelled, a reorientation vector $\hat{\boldsymbol{r}}(\boldsymbol{s},t)$ is computed that maps the location $\boldsymbol{r}$ in the reoriented region (at time t) to the corresponding location $\boldsymbol{s}$ in the reference fundamental region (at time $t=0$) as shown in Fig. 1. With this notation, the ODF can either be represented as $\mathscr{A}(\boldsymbol{r},t)$ (Eulerian form) or $\widehat{\mathscr{A}}(\boldsymbol{s},t)$ (Lagrangian form) with the two representations related as: $\mathscr{A}(\boldsymbol{r},t)=\mathscr{A}(\hat{\boldsymbol{r}}(\boldsymbol{s},t),t)=\widehat{\mathscr{A}}(\boldsymbol{s},t)$.

In this work, the Lagrangian version of the ODF conservation equation is used to compute the ODF at any time, t, during deformation using the following equation (Kumar and Dawson, 1996, 1997):

$$\widehat{\mathscr{A}}(\boldsymbol{s},t)J(\boldsymbol{s},t)=\widehat{\mathscr{A}}(\boldsymbol{s},0)=\mathscr{A}_0(\boldsymbol{s}), \tag{1}$$

where $J(\boldsymbol{s},t)=\det(\nabla\hat{\boldsymbol{r}}(\boldsymbol{s},t))$ is the Jacobian determinant of the reorientation of crystals and $\widehat{\mathscr{A}}(\boldsymbol{s},0)=\mathscr{A}_0(\boldsymbol{s})$ is the initial texturing of the material.

The polycrystal average of an orientation dependent property, $\boldsymbol{\Upsilon}(\boldsymbol{r},t)$, is determined as

$$\langle\boldsymbol{\Upsilon}\rangle=\int_{\mathscr{R}_t}\boldsymbol{\Upsilon}(\boldsymbol{r},t)\mathscr{A}(\boldsymbol{r},t)\,\mathrm{d}v_t=\int_{\mathscr{R}}\boldsymbol{\Upsilon}(\hat{\boldsymbol{r}}(\boldsymbol{s},t),t)\mathscr{A}_0(\boldsymbol{s})\,\mathrm{d}v, \tag{2}$$

where $\mathrm{d}v_t$ is a volume element in the reoriented region.

2.1. Single-crystal constitutive problem

We shall employ the (now) classical single-crystal plasticity theory (e.g., Taylor, 1938; Mandel, 1965; Rice, 1971; Mandel, 1972; Hill, 1965; Teodosiu and Sidoroff, 1976; Asaro, 1983; Asaro and Needleman, 1985; Rashid and Nemat-Nasser, 1990; Bronkhorst et al., 1992; Cuitiño and Ortiz, 1992) based on the notion that plastic flow takes place through slip on prescribed slip systems. A rate-independent version of the single-crystal plasticity

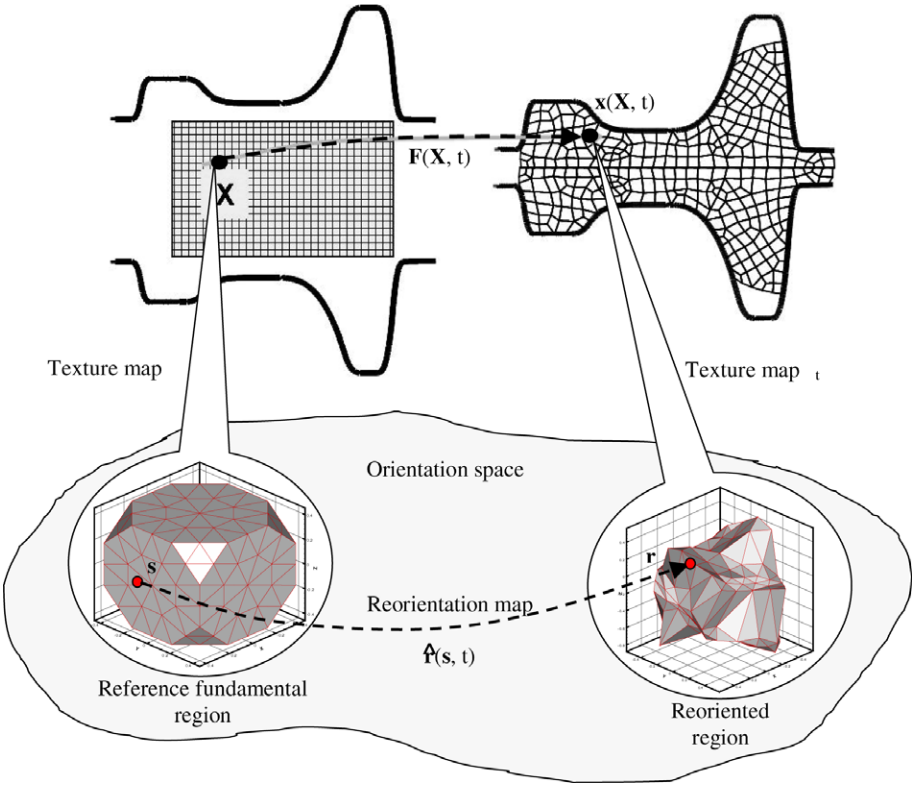

Fig. 1. A Lagrangian framework describing texture development at a material point $\boldsymbol{X}$ using parameters $\boldsymbol{s}$ and $\boldsymbol{r}$, drawn from the RF fundamental region.

model developed in Anand and Kothari (1996) is used to model the single-crystal constitutive response and is summarized below.

For a material with $\alpha = 1, \ldots, N$ slip systems defined by ortho-normal vector pairs $(\boldsymbol{m}^\alpha, \boldsymbol{n}^\alpha)$ denoting the slip direction and slip plane normal respectively, the constitutive equations relate the following basic fields: the Cauchy stress $\boldsymbol{T}$, the slip resistances $s^\alpha > 0$ and the deformation gradient $\boldsymbol{F}$ which can be decomposed into elastic and plastic parts as $\boldsymbol{F} = \boldsymbol{F}^{\mathrm{e}}\,\boldsymbol{F}^{\mathrm{p}}$ with $\det \boldsymbol{F}^{\mathrm{p}} = 1$. In the constitutive equations (intended to characterize small elastic strains) to be defined below, the Green elastic strain measure $\overline{\boldsymbol{E}}^{\mathrm{e}} = \frac{1}{2}(\boldsymbol{F}^{\mathrm{e}T}\boldsymbol{F}^{\mathrm{e}} - \boldsymbol{I})$ defined on the relaxed configuration (plastically deformed, unstressed configuration) $\overline{\mathscr{B}}$ is utilized. The conjugate stress measure is then defined as $\overline{\boldsymbol{T}} = \det \boldsymbol{F}^{\mathrm{e}} (\boldsymbol{F}^{\mathrm{e}})^{-1} \boldsymbol{T} (\boldsymbol{F}^{\mathrm{e}})^{-T}$ where $\boldsymbol{T}$ is the Cauchy stress for the crystal in the sample reference frame.

The constitutive relation, for stress, is given by $\overline{\boldsymbol{T}} = \mathscr{L}^{\mathrm{e}}[\overline{\boldsymbol{E}}^{\mathrm{e}}]$ where $\mathscr{L}^{\mathrm{e}}$ is the fourth-order anisotropic elasticity tensor. It is assumed that deformation takes place through dislocation glide and the evolution of the plastic flow is given by

$$\boldsymbol{L}^{\mathrm{p}} = \dot{\boldsymbol{F}}^{\mathrm{p}} (\boldsymbol{F}^{\mathrm{p}})^{-1} = \sum_{\alpha} \dot{\gamma}^\alpha \boldsymbol{S}_0^\alpha \mathrm{sign}(\tau^\alpha), \tag{3}$$

where $\boldsymbol{S}_0^\alpha = \boldsymbol{m}^\alpha \otimes \boldsymbol{n}^\alpha$ is the Schmid tensor and $\dot{\gamma}^\alpha$ is the plastic shearing rate on the αth slip system. The resolved stress on the αth slip system is given by $\tau^\alpha = \overline{\boldsymbol{T}} \cdot \boldsymbol{S}_0^\alpha$. The resolved

shear stress τ^α attains a critical value s^α on the systems where slip occurs ($\dot{\gamma}^\alpha > 0$). Further, the resolved shear stress does not exceed s^α on the inactive systems with $\dot{\gamma}^\alpha = 0$. The hardening law for the slip resistance s^α is taken as

$$\dot{s}^\alpha(t) = \sum_\beta h^{\alpha\beta}\dot{\gamma}^\beta, s^\alpha(0) = s_0^\alpha. \tag{4}$$

A constitutive time-integration procedure for the rate-independent crystal plasticity model is detailed in Anand and Kothari (1996). The constitutive problem is solved at every integration point in a reference fundamental region attached to a macroscopic material point.

For computing texture evolution, the reorientation velocity for use in Eq. (1) is found as follows:

$$\boldsymbol{v} = \frac{\partial \boldsymbol{r}}{\partial t} = \frac{1}{2}(\boldsymbol{\omega} + (\boldsymbol{\omega}\cdot\boldsymbol{r})\boldsymbol{r} + \boldsymbol{\omega}\times\boldsymbol{r}), \tag{5}$$

where $\boldsymbol{r}$ is the orientation (Rodrigues' parametrization) and $\boldsymbol{\omega}$ represents the spin vector defined as $\boldsymbol{\omega} = \text{vect}(\dot{\boldsymbol{R}}^e\boldsymbol{R}^{eT}) = \text{vect}(\boldsymbol{\Omega})$ where $\boldsymbol{R}^e$ is evaluated through the polar decomposition of the elastic deformation gradient $\boldsymbol{F}^e$ as $\boldsymbol{F}^e = \boldsymbol{R}^e\boldsymbol{U}^e$.

2.2. Solution of the kinematic problem

We follow an updated Lagrangian formulation to solve the direct deformation problem in a generic forming stage in which material occupying an initial configuration $\boldsymbol{B}_0$ is deformed to obtain a configuration $\boldsymbol{B}_{n+1}$ at time $t = t_{n+1}$. Using an updated Lagrangian framework, the total deformation gradient $\boldsymbol{F}$ at time $t = t_{n+1}$ can be expressed in terms of $\boldsymbol{F}_n$ at time $t = t_n$ as $\boldsymbol{F} = \boldsymbol{F}_r\boldsymbol{F}_n$, where $\boldsymbol{F}_r$ is the relative deformation gradient. In the absence of body forces, the equilibrium equation at $t = t_{n+1}$ can be expressed in the reference configuration $\boldsymbol{B}_n$ as

$$\nabla_n \cdot \langle \boldsymbol{P}_r \rangle = 0, \tag{6}$$

where ∇_n denotes the divergence in $\boldsymbol{B}_n$. The polycrystal-averaged Piola–Kirchhoff I stress $\langle \boldsymbol{P}_r \rangle$ is expressed per unit area of $\boldsymbol{B}_n$ and given in terms of the average Cauchy stress ($\langle \boldsymbol{T} \rangle$) as $\langle \boldsymbol{P}_r \rangle = \det\boldsymbol{F}_r \langle \boldsymbol{T} \rangle \boldsymbol{F}_r^{-T}$ using the Taylor hypothesis for the macro–micro linking assumption. The solution of the deformation problem in the current processing stage proceeds incrementally in time starting from the initial configuration $\boldsymbol{B}_0$. Each increment involves the solution of the virtual work equation given by

$$\int_{\boldsymbol{B}_n} \langle \boldsymbol{P}_r \rangle \cdot \nabla_n \tilde{\boldsymbol{u}} \, \mathrm{d}V_n = \int_{\Gamma_n} \boldsymbol{t}\cdot\tilde{\boldsymbol{u}} \, \mathrm{d}A_n, \tag{7}$$

where the test displacement $\tilde{\boldsymbol{u}}$ is expressed over the initial configuration $\boldsymbol{B}_n$. The right hand side term in the above equation involves implicit traction conditions as a result of contact between surfaces. The contact problem is solved using an augmented Lagrangian framework detailed for 2D deformation in Srikanth and Zabaras (2000) and 3D deformation in Acharjee and Zabaras (2006). To solve this non-linear equation, a Newton–Raphson iterative scheme along with a line search procedure is employed. The fully implicit linearization scheme for the micro-averaged PK-I stress is presented in Sundararaghavan (2007) and is not repeated for brevity.

3. Continuum sensitivity method for microstructure-sensitive design

Deformation process design for desired material properties has for long been empirical in nature. Such approaches are not only time consuming but also quite costly. With these issues in mind, in this section, an efficient framework is developed for computational design of deformation processes for desired microstructure-sensitive properties.

The design framework adopted here is based on a gradient optimization method. To calculate the gradients of the objective function and constraints, one needs to calculate the sensitivities, i.e. change in the property to be controlled due to infinitesimal perturbations to the design parameters. The sensitivities are evaluated using the continuum sensitivity method (CSM). In this method, sensitivities are exactly defined using a set of field equations developed by directly differentiating the equations of the direct deformation problem with respect to the macro-scale process parameters. For example, sensitivity of the equilibrium equation is considered to establish a principle of virtual work like equation for obtaining sensitivity of macro-scale deformation fields. A CSM-based gradient optimization approach has been used previously to solve design problems for optimum process parameters and preform shapes in metal forming applications using phenomenological models (Badrinarayanan and Zabaras, 1996; Srikanth and Zabaras, 2001; Ganapathysubramanian and Zabaras, 2002; Acharjee and Zabaras, 2006). In this paper, the technique is applied for the first time to multi-scale design problems. New developments include the use of averaging relations to compute sensitivity of stress and various material properties at the macroscopic level from computed microstructural sensitivity fields. Conventional forming design problems solely address macro-scale objectives such as maximization of die cavity fill and minimization of material wastage in the form of flash (Srikanth and Zabaras, 2001; Chenot et al., 1996; Zhao et al., 1997; Sousa et al., 2002). This paper, in addition to optimizing these objectives, also addresses optimization of variations in material properties that depend on the underlying microstructure. The approach is explained in detail in this section.

3.1. Sensitivity of deformation problem

Let us consider the sensitivities with respect to the design parameters $\boldsymbol{\beta}$ of field variables in the current forming stage. Such typical process parameters may include the ram speed history, the die surface of the current stage, and others. An updated Lagrangian representation is adopted here. Let us consider a generic field Φ that can represent $\boldsymbol{x}$ or any other material or deformation related field. The dependence of the updated Lagrangian field $\Phi = \widehat{\Phi}(\boldsymbol{x}_n, t; \boldsymbol{\beta})$ on $\boldsymbol{\beta}$ can be expressed as follows:

$$\Phi = \widehat{\Phi}(\boldsymbol{x}_n, t; \boldsymbol{\beta}) = \widehat{\Phi}(\tilde{\boldsymbol{x}}(\boldsymbol{X}, t; \boldsymbol{\beta}), t; \boldsymbol{\beta}) = \widetilde{\Phi}(\boldsymbol{X}, t; \boldsymbol{\beta}) \tag{8}$$

with the position $\boldsymbol{x}_n$ referred to the reference configuration $\boldsymbol{B}_n$. The parameter sensitivity $\overset{\circ}{\Phi} = \overset{\circ}{\widehat{\Phi}}(\boldsymbol{x}_n, t; \boldsymbol{\beta}, \Delta\boldsymbol{\beta})$ is defined as the total Gateaux differential of $\Phi = \widehat{\Phi}(\boldsymbol{x}_n, t; \boldsymbol{\beta})$ in the direction $\Delta\boldsymbol{\beta}$ computed at $\boldsymbol{\beta}$:

$$\overset{\circ}{\widehat{\Phi}}(\boldsymbol{x}_n, t; \boldsymbol{\beta}, \Delta\boldsymbol{\beta}) = \frac{\mathrm{d}}{\mathrm{d}\lambda} \widetilde{\Phi}(\boldsymbol{X}, t; \boldsymbol{\beta} + \lambda\Delta\boldsymbol{\beta})|_{\lambda=0}. \tag{9}$$

Extension of these definitions to shape sensitivities (e.g. sensitivities with respect to the preform shape) is a mathematically more complex process that is described in detail in Srikanth and Zabaras (2000).

The novelty in this paper is that the definitions for sensitivity fields are now extended towards a multi-length scale framework. The process of evaluating the sensitivities of fields on the micro-scale due to perturbations on the macro-scale is shown schematically in Fig. 2. This requires a macro-sensitivity problem where the interest is to compute how perturbations on the macro-design variables $\boldsymbol{\beta}$ affect the continuum fields – the deformation gradient $\boldsymbol{F}$ and the velocity gradient $\boldsymbol{L}$. The dependence of the deformation gradient $\boldsymbol{F}$ on $\boldsymbol{\beta}$, in a total Lagrangian framework, can be expressed as $\boldsymbol{F} = \boldsymbol{F}(\boldsymbol{X}, t; \boldsymbol{\beta})$. The parameter sensitivity $\overset{\circ}{\boldsymbol{F}} = \overset{\circ}{\boldsymbol{F}}(\boldsymbol{X}, t; \boldsymbol{\beta}, \Delta\boldsymbol{\beta})$ is defined as the total Gateaux differential of the deformation gradient in the direction $\Delta\boldsymbol{\beta}$ computed at $\boldsymbol{\beta}$:

$$\overset{\circ}{\boldsymbol{F}}(\boldsymbol{X}, t; \boldsymbol{\beta}, \Delta\boldsymbol{\beta}) = \frac{\mathrm{d}}{\mathrm{d}\lambda}\boldsymbol{F}(\boldsymbol{X}, t; \boldsymbol{\beta} + \lambda\Delta\boldsymbol{\beta})\Big|_{\lambda=0}. \tag{10}$$

The micro-sensitivity problem, also defined in Fig. 2, computes the resulting variation of the ODF and other microstructural properties from the perturbation $\Delta\boldsymbol{F}$ of $\boldsymbol{F}$ (or $\Delta\boldsymbol{L}$ of the velocity gradient $\boldsymbol{L}$). In extending the direct analysis in earlier sections, which was based on the Taylor hypothesis, Taylor hypothesis for the sensitivity problems is developed as well. In particular, this is defined as follows: the sensitivity of the deformation gradient at a material point is taken to be the same as the sensitivity of the deformation gradient of the underlying crystals, in the sample reference frame. Before the sensitivity

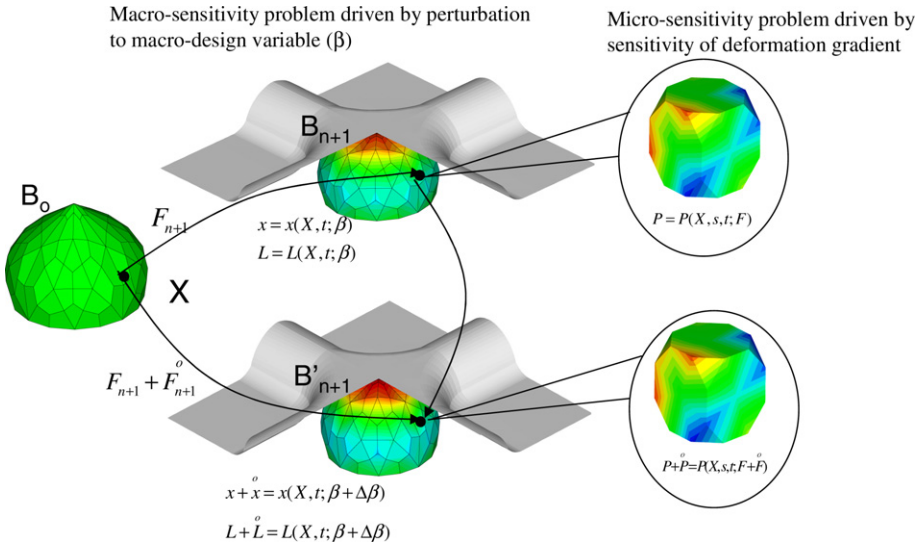

Fig. 2. Pictorial of the two-length scale sensitivity analysis. On the left, the macro-sensitivity problem (following a Lagrangian approach) computes the sensitivities of continuum fields (e.g. of the velocity gradient) with respect to macro-design variables (here the die surface). On the right, the micro-sensitivity problem computes the sensitivity of the ODF at each material point with respect to perturbations in deformation gradient induced by the die shape perturbation.

problems are discussed, the polycrystal average of sensitivity fields needs to be defined. This is defined as follows:

$$\langle \overset{\circ}{\boldsymbol{\Upsilon}} \rangle = \overline{\overset{\circ}{\int_{\mathscr{R}_t} \boldsymbol{\Upsilon}(\boldsymbol{r},t;\boldsymbol{\beta})\mathscr{A}(\boldsymbol{r},t;\boldsymbol{\beta})\,\mathrm{d}v_t}} = \int_{\mathscr{R}} \overset{\circ}{\boldsymbol{\Upsilon}}(\hat{\boldsymbol{r}}(\boldsymbol{s},t;\boldsymbol{\beta}),t;\boldsymbol{\beta},\Delta\boldsymbol{\beta})\mathscr{A}_0(\boldsymbol{s})\,\mathrm{d}v$$
$$= \int_{\mathscr{R}} \widehat{\overset{\circ}{\boldsymbol{\Upsilon}}}(\boldsymbol{s},t;\boldsymbol{\beta},\Delta\boldsymbol{\beta})\mathscr{A}_0(\boldsymbol{s})\,\mathrm{d}v, \tag{11}$$

where $\mathrm{d}v_t$ is defined as the volume element on the reoriented region and it is assumed that the initial texture is fixed (i.e. $\overset{\circ}{\mathscr{A}}_0 = 0$). From Eq. (11), one can conclude that at no point in the analysis, the sensitivity of the ODF is needed to compute the polycrystal average of different properties. Examples discussed later, however, do report the sensitivity of the ODF as a post-processing step for validating the developed analysis.

Described below is the analysis for the development of an updated Lagrangian sensitivity formulation for the deformation problem. In this approach, the governing equations of the various sub-problems in the direct analysis (e.g. the kinematic, constitutive, contact analysis) are first design-differentiated and then appropriate weak forms, time integration and discretization are introduced. The resulting linear sensitivity sub-problems are combined to produce a linear problem for computing the sensitivity of the deformation, plastic deformation gradient and material state.

The sensitivity deformation problem is developed on the reference preform $\boldsymbol{B}_n$. The design sensitivity of the equilibrium equation (Eq. (6)) at $t = t_{n+1}$ results in

$$\overline{\overset{\circ}{\nabla_{n\cdot}\langle \boldsymbol{P}_r \rangle}} = 0, \quad \forall\ \boldsymbol{x}_n \in \boldsymbol{B}_n. \tag{12}$$

A variational form for the above sensitivity equilibrium equation can be posed as follows (Srikanth and Zabaras, 2000):

$$\int_{\boldsymbol{B}_n} \langle \overset{\circ}{\boldsymbol{P}}_r \rangle \cdot \nabla_n \tilde{\boldsymbol{\eta}}\,\mathrm{d}V_n - \int_{\boldsymbol{B}_n} (\langle \boldsymbol{P}_r \rangle [\nabla_n \cdot \boldsymbol{L}_n^T]) \cdot \tilde{\boldsymbol{\eta}}\,\mathrm{d}V_n - \int_{\boldsymbol{B}_n} (\langle \boldsymbol{P}_r \rangle \boldsymbol{L}_n^T) \cdot \nabla_n \tilde{\boldsymbol{\eta}}\,\mathrm{d}V_n$$
$$= \int_{\boldsymbol{\Gamma}_n} \{\overset{\circ}{\boldsymbol{\lambda}} - [\boldsymbol{L}_n \cdot (\boldsymbol{N} \otimes \boldsymbol{N})]\boldsymbol{\lambda}\} \cdot \tilde{\boldsymbol{\eta}}\,\mathrm{d}A_n, \tag{13}$$

where $\tilde{\boldsymbol{\eta}}$ is a kinematically admissible sensitivity deformation field expressed over the reference configuration $\boldsymbol{B}_n$, $\boldsymbol{N}$ is the unit normal vector to $\boldsymbol{\Gamma}_n$ and the (known) design velocity gradient $\boldsymbol{L}_n$ at t_n is defined as follows:

$$\boldsymbol{L}_n \equiv \nabla_n \widehat{\overset{\circ}{\boldsymbol{x}}}(\boldsymbol{x}_{n-1}, t_n; \boldsymbol{\beta}, \Delta\boldsymbol{\beta}) = \overset{\circ}{\boldsymbol{F}}_n \boldsymbol{F}_n^{-1}. \tag{14}$$

The primary unknown of Eq. (13) is the design differential $\overset{\circ}{\boldsymbol{x}}_{n+1} = \widehat{\overset{\circ}{\boldsymbol{x}}}(\boldsymbol{x}_n, t_{n+1}; \boldsymbol{\beta}, \Delta\boldsymbol{\beta})$. To obtain the final form of the variational sensitivity problem, the relationships between $\overset{\circ}{\boldsymbol{F}}_r$, $\langle \overset{\circ}{\boldsymbol{P}}_r \rangle$ and $\overset{\circ}{\boldsymbol{\lambda}}$ to $\overset{\circ}{\boldsymbol{x}}_{n+1}$ need to be developed.

The relationship between $\overset{\circ}{\boldsymbol{F}}_r$ and $\overset{\circ}{\boldsymbol{x}}_{n+1}$ is purely kinematic and is given as follows:

$$\overset{\circ}{\boldsymbol{F}}_r = \overline{\overset{\circ}{\nabla_n \boldsymbol{x}_{n+1}}} = \nabla_n \overset{\circ}{\boldsymbol{x}}_{n+1} - \boldsymbol{F}_r \boldsymbol{L}_n. \tag{15}$$

The relationship between $\overset{\circ}{\boldsymbol{\lambda}}$ and $\overset{\circ}{\boldsymbol{x}}_{n+1}$ is obtained from the sensitivity contact problem as

$$\overset{\circ}{\boldsymbol{\lambda}} = \boldsymbol{D}[\overset{\circ}{\boldsymbol{x}}_{n+1}] + \boldsymbol{d}, \tag{16}$$

where $\boldsymbol{D}$ is a second-order tensor and $\boldsymbol{d}$ a vector. The non-trivial derivation of these tensors resulting by design-differentiation of a regularized contact problem can be found in Srikanth and Zabaras (2000).

The relationship between $\langle \overset{\circ}{\boldsymbol{P}}_r \rangle$ and $\overset{\circ}{\boldsymbol{x}}_{n+1}$ is obtained from the sensitivity constitutive problem and takes the form:

$$\langle \overset{\circ}{\boldsymbol{P}}_r \rangle = \mathscr{A}[\overset{\circ}{\boldsymbol{F}}_r] + \boldsymbol{B}, \tag{17}$$

where $\mathscr{A}$ is a fourth-order tensor and $\boldsymbol{B}$ is a second-order tensor. Analogous to the constitutive update for the direct deformation problem, the sensitivity constitutive update procedure involves computation of the set $\overset{\circ}{\boldsymbol{T}}, \overset{\circ}{s}, \overset{\circ}{\boldsymbol{F}}^{\mathrm{e}}, \overset{\circ}{\boldsymbol{F}}^{\mathrm{p}}$ for each crystal orientation at the end of the time increment t_{n+1}, where the sensitivity of the total deformation gradient $\overset{\circ}{\boldsymbol{F}}_{n+1}$ is assumed known. The detailed derivations of the sensitivity constitutive equations can be found in Sundararaghavan (2007).

The constitutive sensitivity problem for a crystal orientation is history-dependent and the solution of the sensitivity problem at time t_n is assumed known for each crystal orientation, yielding the variables $\overset{\circ}{s}_n, \overset{\circ}{\boldsymbol{F}}^{\mathrm{e}}_n, \overset{\circ}{\boldsymbol{F}}^{\mathrm{p}}_n$ at the beginning of each time increment. The active systems identified in the direct problem are then used for deriving the sensitivity of these quantities at the current time step. This assumes that slip systems activated under a perturbed deformation gradient $(\boldsymbol{F} + \overset{\circ}{\boldsymbol{F}})$ are the same as when a deformation gradient of $\boldsymbol{F}$ is acting on the crystal. This is a valid assumption since the applied perturbations to the design variables are small ($\sim 10^{-7}$) and hence, no new slip systems are activated.

The post-processing step involves computation of the sensitivity of the orientation distribution function at each material point in the macro-continuum. For this, one needs to first compute the sensitivity of the reorientation vector. Once $\overset{\circ}{\boldsymbol{F}}^{\mathrm{e}}_{n+1}$ has been evaluated using the sensitivity constitutive problem, $\overset{\circ}{\boldsymbol{R}}^{\mathrm{e}}_{n+1}$ can be obtained as (Badrinarayanan and Zabaras, 1996) (the subscript $n+1$ is dropped in this equation):

$$\overset{\circ}{\boldsymbol{R}}^{\mathrm{e}} = \overset{\circ}{\boldsymbol{F}}^{\mathrm{e}} \boldsymbol{F}^{\mathrm{e}-1} \boldsymbol{R}^{\mathrm{e}} - \boldsymbol{R}^{\mathrm{e}} \mathrm{sym}\{\boldsymbol{U}^{\mathrm{e}-1} \mathrm{sym}(\boldsymbol{F}^{\mathrm{e}T} \overset{\circ}{\boldsymbol{F}}^{\mathrm{e}})\} \boldsymbol{F}^{e-1} \boldsymbol{R}^{\mathrm{e}}. \tag{18}$$

The sensitivities of the spin vector and the spin tensor are obtained as

$$\overset{\circ}{\boldsymbol{\omega}} = \mathrm{vect}(\overset{\circ}{\boldsymbol{\Omega}}), \quad \text{where } \overset{\circ}{\boldsymbol{\Omega}} = \dot{\overset{\circ}{\boldsymbol{R}}}^{\mathrm{e}} \boldsymbol{R}^{\mathrm{e}T} - \boldsymbol{\Omega} \overset{\circ}{\boldsymbol{R}}^{\mathrm{e}} \boldsymbol{R}^{\mathrm{e}T}. \tag{19}$$

The sensitivity of the reorientation vector $\overset{\circ}{\boldsymbol{r}}_{n+1}$ can now be found by design differentiating and solving Eq. (5). Design-differentiation of the Lagrangian version of the ODF conservation equation (Eq. (1)), leads to the following equation for the sensitivity of the ODF:

$$\overset{\circ}{\widehat{\mathscr{A}}}(\boldsymbol{s}, t; \boldsymbol{\beta}, \Delta\boldsymbol{\beta}) J(\boldsymbol{s}, t; \boldsymbol{\beta}) = -\widehat{\mathscr{A}}(\boldsymbol{s}, t; \boldsymbol{\beta}) \overset{\circ}{J}(\boldsymbol{s}, t; \boldsymbol{\beta}, \Delta\boldsymbol{\beta}), \tag{20}$$

where $\overset{\circ}{J}(\boldsymbol{s}, t; \boldsymbol{\beta}, \Delta\boldsymbol{\beta}) = \overset{\circ}{\det(\nabla \hat{\boldsymbol{r}}(\boldsymbol{s}, t; \boldsymbol{\beta}, \Delta\boldsymbol{\beta}))} = J(\boldsymbol{s}, t; \boldsymbol{\beta})[\nabla \cdot \overset{\circ}{\boldsymbol{r}}(\boldsymbol{s}, t; \boldsymbol{\beta}, \Delta\boldsymbol{\beta})]$.

3.2. Definition of the gradient optimization problem

Using the computed sensitivity fields, one can evaluate the gradients of any microstructure-dependent property $\langle \Upsilon \rangle$ with respect to the components of a design vector $\boldsymbol{\beta}$ of size m. The design vector $\boldsymbol{\beta}$ can be an appropriate parametrization of the macro-scale design variable that can represent the die or preform shape, forging velocity, etc. The gradient is represented as $\nabla \langle \Upsilon \rangle = \left(\frac{\partial \langle \Upsilon \rangle}{\partial \beta_1}, \frac{\partial \langle \Upsilon \rangle}{\partial \beta_2}, \ldots, \frac{\partial \langle \Upsilon \rangle}{\partial \beta_m} \right)$ where

$$\frac{\partial\langle\boldsymbol{\Upsilon}\rangle}{\partial\beta_i} = \frac{\overset{\circ}{\langle\boldsymbol{\Upsilon}\rangle}(\boldsymbol{r}, t; \beta_1, \ldots, \beta_m, 0, \ldots, \Delta\beta_i, \ldots, 0)}{\Delta\beta_i}. \tag{21}$$

The ith sensitivity problem is driven by $\Delta\beta_i$ with $\Delta\beta_j = 0$ for $j \neq i$.

The objective function for the gradient optimization problem where it is desirable to obtain a set of properties $\langle\boldsymbol{\Upsilon}\rangle^{\text{desired}}$ can be as follows:

$$\min_{\boldsymbol{\beta}} \boldsymbol{F}(\boldsymbol{\beta}) = \frac{1}{2N}\sum_{i=1}^{N}(\langle\boldsymbol{\Upsilon}\rangle_i(\boldsymbol{\beta}) - \langle\boldsymbol{\Upsilon}\rangle_i^{\text{desired}})^2, \tag{22}$$

where N is the total number of sampling points (for e.g. nodal points of interest in the final macro-scale mesh) and $\langle\boldsymbol{\Upsilon}\rangle_i$ defines the property computed at the ith sampling point. Alternately, the objective function can be expressed in vector notation as

$$\min_{\boldsymbol{\beta}} \boldsymbol{F}(\boldsymbol{\beta}) = \frac{1}{2N}(\Delta\langle\boldsymbol{\Upsilon}\rangle)^T(\Delta\langle\boldsymbol{\Upsilon}\rangle), \tag{23}$$

where $\Delta\langle\boldsymbol{\Upsilon}\rangle = \langle\boldsymbol{\Upsilon}\rangle(\boldsymbol{\beta}) - \langle\boldsymbol{\Upsilon}\rangle^{\text{desired}}$. An iterative approach is followed to solve for $\boldsymbol{\beta}$ which would give the desired property. Let $\boldsymbol{\beta}^r$ be the solution at the rth optimization iteration step. The descent direction $\boldsymbol{d}^r$ of $\boldsymbol{F}(\boldsymbol{\beta})$ can be computed from Eq. (23) as

$$\boldsymbol{d}^r = -\nabla_\beta \boldsymbol{F}(\boldsymbol{\beta}) = -\frac{1}{N}\boldsymbol{S}_{\beta^r}^T(\Delta\langle\boldsymbol{\Upsilon}\rangle), \tag{24}$$

where the sensitivity matrix $\boldsymbol{S}_\beta$ of $\langle\boldsymbol{\Upsilon}\rangle$ is defined as $\boldsymbol{S}_\beta \equiv \partial\langle\boldsymbol{\Upsilon}\rangle/\partial\boldsymbol{\beta}$. $\boldsymbol{S}_\beta$ is of the order $N \times m$, where N is the dimension of $\langle\boldsymbol{\Upsilon}\rangle$ (number of sampling points) and m is the dimension of the design vector $\boldsymbol{\beta}$. After each iteration, the design parameters are updated as follows:

$$\boldsymbol{\beta}^{r+1} = \boldsymbol{\beta}^r + \delta_r \boldsymbol{d}^r, \quad r = 0, 1, \ldots, \tag{25}$$

where the optimal scalar δ_r is computed from a line search procedure:

$$\boldsymbol{F}(\boldsymbol{\beta}^r + \delta_r \boldsymbol{d}^r) = \min_{\delta \geqslant 0} \boldsymbol{F}(\langle\boldsymbol{\Upsilon}(\boldsymbol{\beta}^r)\rangle + \delta\boldsymbol{d}^r) \tag{26}$$

leading to the following step size:

$$\delta = -\frac{\boldsymbol{d}^{rT}\boldsymbol{S}_{\beta^r}^T\Delta\langle\boldsymbol{\Upsilon}\rangle}{\boldsymbol{d}^{rT}\boldsymbol{S}_{\beta^r}^T\boldsymbol{S}_{\beta^r}\boldsymbol{d}^r}. \tag{27}$$

This step size is used to update the design vector and the iterative process is repeated until the prescribed convergence criterion is satisfied.

4. Numerical examples

The slip system hardening model used in the examples is given as

$$h^{\alpha\beta} = [q + (1-q)\delta^{\alpha\beta}]h^\beta \quad (\text{no sum on } \beta), \tag{28}$$

where h^β is a single-slip hardening rate, q is the latent-hardening ratio and $\delta^{\alpha\beta}$ is the Kronecker delta function. The parameter q is taken to be 1.0 for coplanar slip systems and 1.4 for non-coplanar slip systems. For the single-slip hardening rate, the following specific form is adopted:

$$h^{\beta} = h_o \left(1 - \frac{s^{\beta}}{s_s}\right)^{a}, \tag{29}$$

where h_o, a, and s_s are slip hardening parameters taken to be identical for all slip systems, with values $h_o = 180$ MPa,$s_s = 148$ MPa and $a = 2.25$ for FCC copper single crystals. The initial value of slip system resistance is taken as $s_o = 16$ MPa (Anand and Kothari, 1996). Values of elastic parameters for copper crystal are taken as $C_{11} = 170$ GPa,$C_{12} = 124$ GPa and $C_{44} = 75$ GPa. Slip is assumed to occur in the 12 $\{1\,1\,1\}\langle 1\,1\,0\rangle$ slip systems in the FCC crystal. As a validation of the micro-scale texture evolution model, results are compared with the numerical example of Anand and Kothari (1996). The experiment corresponds to an x-axis compression with a strain rate of 0.001 s^{-1} of FCC copper polycrystal. The initial texturing of the material is assumed to be random, and this corresponds to a constant Lagrangian ODF of 2.435. The reference fundamental region is discretized into 448 tetrahedral elements with cubic symmetry enforced in the solution procedure. Comparison of results of Anand and Kothari (1996) with the present ODF-Taylor model is shown in Fig. 3.

To validate the continuum sensitivity algorithm, we consider the problem of plane strain compression of a block and compare the sensitivity of the ODF with respect to the straining rate using the continuum sensitivity method (CSM) and the finite difference method (FDM). The evaluation of the gradient, using CSM in this case, involves solving one non-linear direct problem and a linear sensitivity problem corresponding to perturbation in the strain rate. In comparison, in the finite difference method (FDM), that uses finite differences to approximate the derivatives, one would require a solution of two non-linear direct problems with compression rates β and $\beta + \delta\beta$. The initial block size is taken as 1.0 mm by 1.0 mm. The straining rate is fixed at 10^{-2} s^{-1}, and simulation is for a total time of 3.2 s. Parameter sensitivities are computed with respect to a perturbation of 10^{-7} s^{-1} to the compression rate. Fig. 4 shows comparison of texture sensitivity of the two techniques in the two-scale problem where it is seen that CSM produces exactly the same sensitivity results as the FDM.

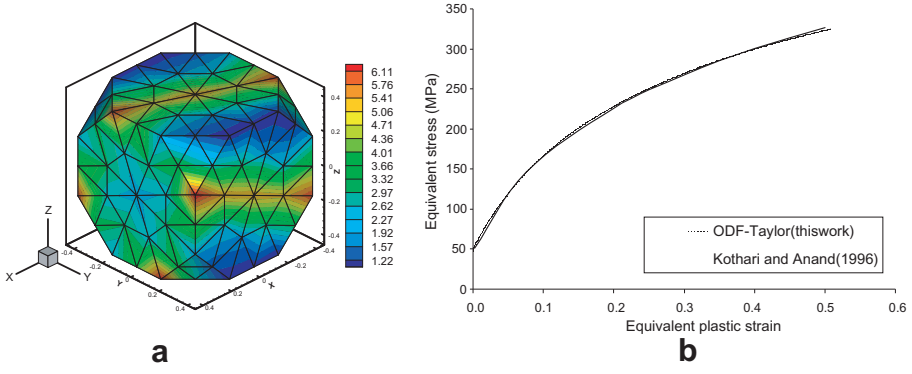

Fig. 3. (a) Texture obtained using the Taylor model after 135 s of simple compression of a copper polycrystal at the rate of 10^{-3} s^{-1}. (b) Comparison of equivalent stress–strain response with results from Anand and Kothari (1996).

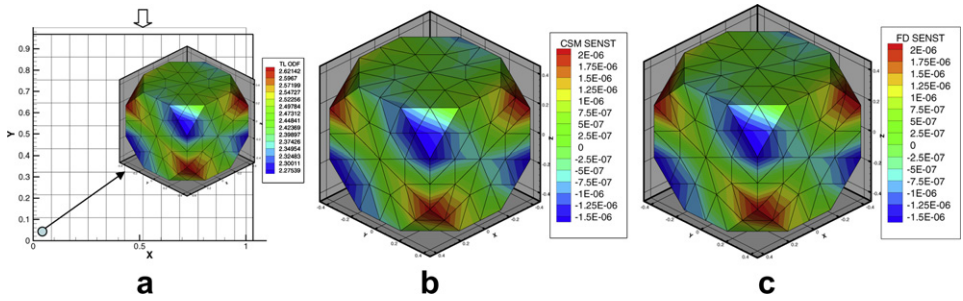

Fig. 4. (a) Multi-scale plane strain compression of a block, final texture at the bottom left corner element is shown. (b) Sensitivity of this texture calculated using the CSM technique is compared with (c) sensitivities obtained using the finite difference technique.

Since the CSM involves solution of a simpler linear sensitivity problem for each design variable, it is much faster than the FDM. The FDM also presents difficulties due to the fact that direct deformation problems, such as those involving abrupt contact between die and the workpiece, are insensitive to infinitesimal changes in design parameters. Further, FDM sensitivities are mesh-dependent and cannot predict accurate sensitivities in problems that involve remeshing operations. On the other hand, accurate sensitivities can be found using CSM with infinitesimal perturbations in deformation/contact problems and the approach works equally well for problems that involve remeshing. Such advantages are important in the case of complex multi-scale deformation problems, and is a factor enabling the proposed algorithm to solve otherwise difficult design examples as demonstrated later in this section.

The parameter sensitivities in the design problem, as discussed later, are computed with respect to a perturbation of 10^{-7} units to the design parameters. First two examples involve control of properties in axi-symmetric extrusion and closed-die forging processes, simulated without remeshing. The last two examples relates to control of strength and magnetic hysteresis losses in complex forging processes in the presence of remeshing and data transfer for both direct and sensitivity fields. In all examples, an assumed strain analysis scheme is used to treat the effect of near-incompressibility based on the work in Srikanth and Zabaras (2001). To aid in speeding up the solution process for the multi-scale problem, the design simulator was parallelized using MPI. The simulator was developed using object oriented programming and was dynamically linked to the parallel toolbox PetSc (Balay et al., 2004) for parallel assembly and solution of linear systems. In particular, for solution of linear systems, a GMRES solver along with block Jacobi and ILU preconditioning from the PetSc toolbox was employed.

4.1. Example 1. Design of Young's modulus distribution during extrusion

In this example, we study the feasibility of controlling Young's Modulus distribution in the finished product through control of the extrusion die shape. An axi-symmetric extrusion process is considered with a fixed reduction in cross section over a fixed length. During extrusion process, texturing and the material state strongly vary over the final cross section due to the loading conditions. Through control of loading conditions, in particular, the die shape, it is possible to minimize variations in properties in the finished product.

The objective is to design the die shape such that Young's modulus distribution at the exit is as uniform as possible. The objective function for this design problem is defined as follows:

$$\min_{\boldsymbol{\beta}} \boldsymbol{F}(\boldsymbol{\beta}) = \sum_{i=1}^{N} ((E_i(\boldsymbol{\beta}) - \overline{E}(\boldsymbol{\beta}))^2), \tag{30}$$

where $E_i (i = 1, \ldots, N)$ is Young's modulus at the N nodal points in the exit cross section and $\overline{E}$ is the mean property over those points defined as $\overline{E} = \frac{1}{N}\sum_{i=1}^{N} E_i$. Young's modulus for loading along a particular direction at each material point is found using the polycrystal stiffness, $\langle \boldsymbol{C} \rangle$, computed through a weighted average (over $\mathscr{A}$) of the stiffness of individual crystals expressed in the sample reference frame. Young's modulus for the polycrystal is then computed through the averaged stiffness matrix as

$$E = \frac{1.0}{(\langle \boldsymbol{C} \rangle^{-1})_{(11)}}. \tag{31}$$

In this example, Young's modulus along the axis of the drawn workpiece was calculated using the above equation but after a coordinate transformation of $\langle \boldsymbol{C} \rangle$ so that the first basis vector is along the extrusion axis.

The initial texture of the preform is assumed to be random, and this corresponds to a constant Lagrangian ODF of 2.435. The reference fundamental region with cubic symmetry is discretized into 61 tetrahedral elements. We design an extrusion process with a die of area reduction of 13.5% over a length of 0.5 mm. Initial radius of the FCC copper workpiece is 0.5 mm and the initial height is 1.0 mm. The workpiece was extruded with a nominal displacement rate of 0.1 s^{-1}. A total of 400 time steps up to $t = 10$ s were performed to reach steady-state conditions at the exit. The die–workpiece interface friction coefficient is taken as 0.01. The die surface is represented by a degree 7 Bézier curve as follows:

$$r(\alpha) = \sum_{i=1}^{7} C_i \phi_i(\alpha), \quad z = \frac{\alpha}{2} \text{ in mm}, \quad 0 \leqslant \alpha \leqslant 1, \tag{32}$$

where $C_i, i = [1, \ldots, 7]$, are the algebraic control parameters. The Bernstein functions $\phi_i(\alpha)$ are given as

$$\begin{aligned} &\phi_1 = (1.0 - \alpha)^6, \quad \phi_2 = 6.0(1.0 - \alpha)^5\alpha, \quad \phi_3 = 15.0(1.0 - \alpha)^4\alpha^2, \\ &\phi_4 = 20.0(1.0 - \alpha)^3\alpha^3, \quad \phi_5 = 15.0(1.0 - \alpha)^2\alpha^4, \\ &\phi_6 = 6.0(1.0 - \alpha)\alpha^5, \quad \phi_7 = \alpha^6. \end{aligned} \tag{33}$$

We apply the constraints (to obtain the same reduction for different die design parameters) that the radius and slope (with respect to the z-axis) at the inlet and exit are fixed with $C_2 = C_1 = 0.52$ mm, $C_6 = C_7 = 0.45$ mm. With this selection of parameters, there are three design parameters $\boldsymbol{\beta} = (C_3, C_4, C_5)$ for the control problem. An initial guess of the design variables of $C_3 = 0.52, C_4 = 0.52, C_5 = 0.52$ mm was employed. The energy and displacement error norms for the finite element solution are taken to be 10^{-4}.

Fig. 5 shows the intermediate configuration (at 0.5 mm stroke) and the final configuration (at 1 mm stroke) of the extrusion process along with a representative ODF (Fig. 5c) obtained at a point on the circumference of the exit cross section at 0.5 mm stroke. Observe that due to the natural symmetry of Rodrigues space, axes of the space relate directly to sample axes. In

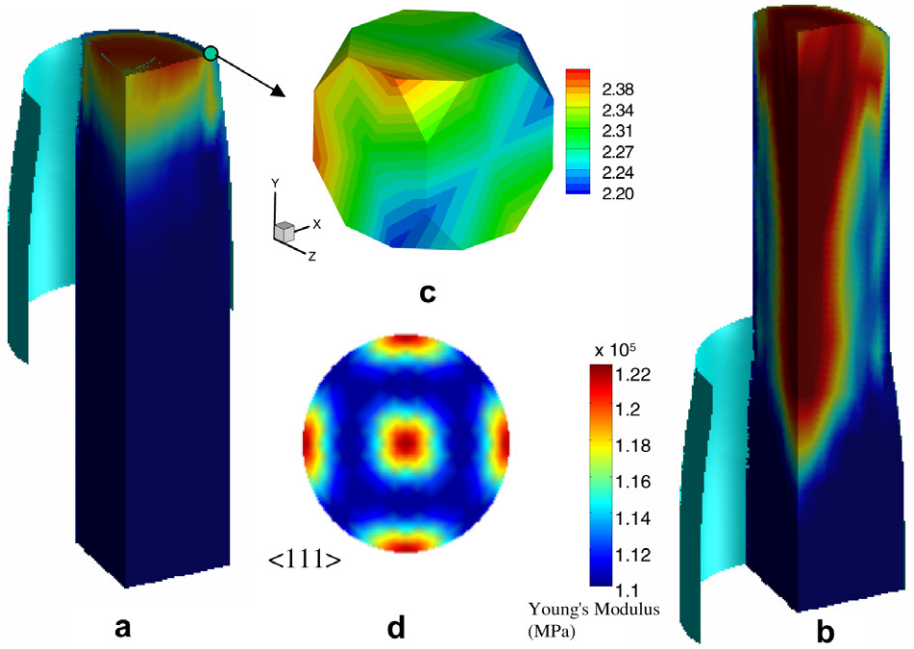

Fig. 5. (a) The distribution of Young's modulus when the exit cross section just leaves the extrusion die (b) Young's modulus distribution in the final time step (c) ODF at a representative material point close to the die surface. (d) The $\langle 1\,1\,1\rangle$ pole figure of the ODF.

axi-symmetric forming operations, we hereafter use the x-direction of the ODF (as indicated in Fig. 5c) to denote the radial (r-)direction and the y-direction of the ODF to denote the axial (z-)sample direction. The ODF, as expected for an extrusion process, can be seen to arise from a predominantly x–y axes shear deformation, as evidenced by the strong x-axis $\langle 1\,1\,1\rangle$ fiber in the $\langle 1\,1\,1\rangle$ pole figure (Fig. 5d). The x-axis $\langle 1\,1\,1\rangle$ fibers lie near boundaries of the fundamental region and are seen across the z-face of the ODF. Note that in Rodrigues–Frank space, ideal orientations lie on boundaries of the fundamental region which allows the structure of the textures to be reflected adequately by the boundary ODF.

The die shape identified at various iterations of the design problem and variation of the objective function over all iterations are shown in Fig. 6. The optimal die shape corresponds to Bézier coefficients $C_3 = 0.5229, C_4 = 0.5099, C_5 = 0.4765$. Young's modulus distribution on the curved surface at the end of forging at the first, second and final iteration are shown in Fig. 7. In the first iteration, Young's modulus distribution is highly non-uniform with variation from 116 GPa at the center to a maximum of 123 GPa halfway from the center. In the final iteration, the deviation reduces to just 1 GPa from the center to about two-thirds of the exit cross section. The optimal solution for the design problem is attained in just four iterations showcasing the efficiency of the design algorithm.

4.2. Example 2. Design of yield strength variation during closed die forging

In this problem, the forging of a circular disc is considered. The primary objective is to design the preform for a final forged product (with fixed stroke) such that the die cavity is

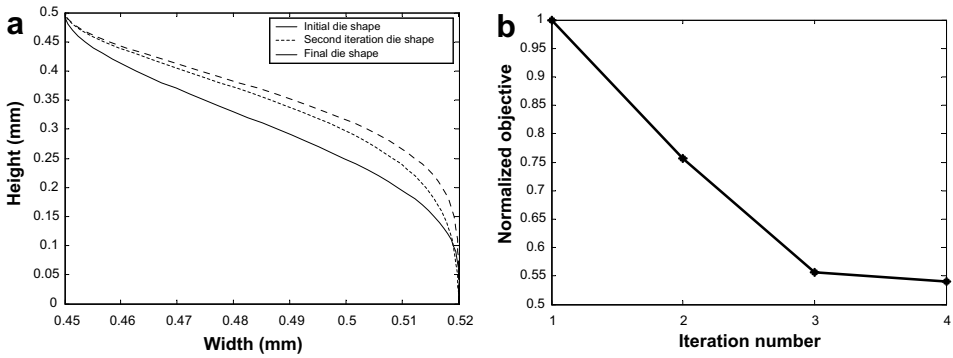

Fig. 6. (a) The extrusion die profile at the initial, intermediate and final (fourth) iteration. (b) The decrease in cost function at successive iterations.

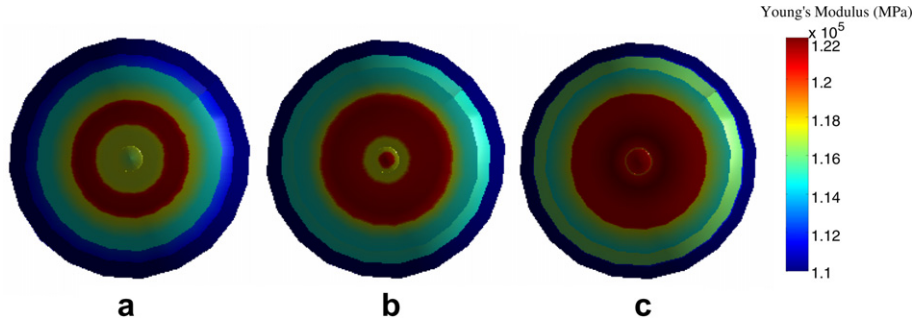

Fig. 7. Young's modulus distribution on the exit cross section at the end of extrusion in the (a) first iteration (b) second iteration (c) final iteration. The workpiece is shown end-on and the outer area depicts material still in the process zone.

fully filled. The secondary objective in this problem is to minimize the variation of strength on the curved surface of the final product. One way to ensure that the die cavity is filled is to consider a preform of a much larger volume than that needed. In this case, the die cavity is filled up but there will be considerable material wastage due to flash. Further, our secondary objective of minimizing yield strength variation might not be satisfied. The objective function for the design problem is defined so as to fulfill both objectives:

$$\min_{\boldsymbol{\beta}} \boldsymbol{F}(\boldsymbol{\beta}) = \frac{1}{N}\sum_{i=1}^{N}((Y_i(\boldsymbol{\beta}) - \overline{Y}(\boldsymbol{\beta}))^2) + \sum_{i=1}^{N^*}((r_i(\boldsymbol{\beta}) - r_i^{\text{desired}})^2 + (z_i(\boldsymbol{\beta}) - z_i^{\text{desired}})^2), \tag{34}$$

where Y_i $(i = 1, \ldots, N)$ are the yield strength values on the curved surface in the final product and $\overline{Y}$ is the mean property over those points defined as $\overline{Y} = \frac{1}{N}\sum_{i=1}^{N} Y_i$. Also, r_i^{desired} and z_i^{desired} are the closest point projections of the points $r_i(\boldsymbol{\beta})$ and $z_i(\boldsymbol{\beta})$ on the die and N^* denotes the number of points on the contact (top and curved) surface. FCC copper is used as the material for the workpiece. The crystal plasticity model described previously is used to calculate the yield strength at all Gauss points using the ODF and slip system resistances at each time step. In this method, the polycrystal at each integration point in

the macro-scale mesh is separately subject to uniaxial (y-axis) tension conditions up to a strain of 0.2% to obtain the corresponding 0.2% offset yield strength at each integration point.

The initial surface of the preform ($R_\beta(\alpha)$) is represented with a degree 6 Bézier curve. Using the restriction $R'_\beta(0) = 0$, the representation of R_β can be defined with 6 independent design variables β_i, $i = [1, \ldots, 6]$ as follows:

$$R_\beta(\alpha) = \sum_{i=1}^{6} \beta_i \phi_i(\alpha), \quad 0 \leqslant \alpha \leqslant 1, \tag{35}$$

where $\alpha = \frac{z}{H}$ represents the z-coordinate normalized with the height of the preform. Basis functions are given as

$$\begin{aligned} &\phi_1 = (1.0-\alpha)^6 + 6\alpha(1-\alpha)^5, \quad \phi_2 = 15.0(1.0-\alpha)^4\alpha^2, \\ &\phi_3 = 20.0(1.0-\alpha)^3\alpha^3, \quad \phi_4 = 15.0(1.0-\alpha)^2\alpha^4, \\ &\phi_5 = 6.0(1.0-\alpha)\alpha^5, \quad \phi_6 = \alpha^6. \end{aligned} \tag{36}$$

The optimization iterations start with a preform of lesser volume than the die cavity and the design iterations try to attain the optimum shape of the final preform that satisfies the objectives. The specified forging velocity is taken as 0.01 mm/s and the shape parameters in the reference preform are $\beta_i = 1.0$ for all i. This corresponds to a cylindrical preform of radius 1.0 mm. The objective is to design the free surface (represented by the degree 6 Bézier curve) of the preform of fixed height $H = 0.60$ mm that when forged using the closed forming die results in a fully-filled die cavity and uniform distribution of yield strength on the external surface after a specified stroke of 0.3 mm. The die is described as follows:

$$\begin{aligned} &r(\eta) = 1.3(1-\eta), \\ &z(\eta) = 548.357\eta^3 + 1.35, \quad \eta \in [0, 0.07692], \\ &z(\eta) = 378.373(\eta - 0.16952)^3 + 1.9, \quad \eta \in [0.07692, 0.16952], \\ &z(\eta) = 1.9, \quad \eta \in [0.16952, 0.36663], \\ &z(\eta) = 0.15(15.0463 - 79.3599\eta + 295.8557\eta^2 - 511.8711\eta^3 + 403.3830\eta^4 \\ &\qquad - 118.0541\eta^5) + 0.85, \quad \eta > 0.36663. \end{aligned} \tag{37}$$

The workpiece is assumed to be isothermal. The initial temperature of the workpiece is assumed to be uniform and equal to 300 K. The forging die is modelled as a rigid surface and to simulate sticking friction between the die and workpiece, a coefficient of friction of 0.1 is applied. The energy and displacement error norms for the finite element solution are taken to be 10^{-4}.

Fig. 8 shows an intermediate step (at 0.02 mm stroke) and the final forged product (at 0.3 mm stroke) at the optimal preform shape along with a representative ODF calculated at the material point marked in the figure. The development of y-axis compression texture is clearly captured in the simulation. FCC metals are typically associated with texturing to $\langle 1\,1\,0 \rangle$ fibers under compression. At lower strain (0.02 mm stroke, Fig. 8c), intensities can be seen to develop uniformly along the compression (y-)axis $\langle 1\,1\,0 \rangle$ fibers that are seen across the z- and x-faces of the ODF. At higher strains (0.3 mm stroke, Fig. 8d), the ODF within the attracting regions about the $\langle 1\,1\,0 \rangle$ fibers intensifies and sharpens. Also, note the boundary symmetry of the space that implies that structures associated with fibers

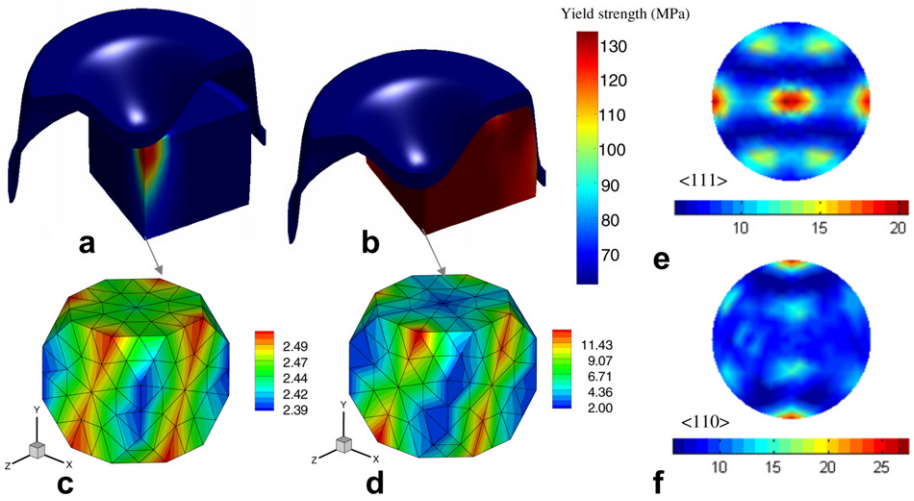

Fig. 8. (a) Yield strength distribution at 0.02 mm stroke. (b) Yield strength distribution at 0.3 mm stroke. (c, d) ODF at a point close to the bottom corner of the preform at 0.02 and 0.3 mm stroke. (e, f) The $\langle 1\,1\,1\rangle$ and $\langle 1\,1\,0\rangle$ pole figures of the ODF in (d).

on opposing faces comprise a single feature. While the $\langle 1\,1\,0\rangle$ fibers correspond to regions attracting crystal flow, the $\langle 1\,0\,0\rangle$ and $\langle 1\,1\,1\rangle$ fibers define regions that repel crystal flow. This is seen from the pole figures in Fig. 8e, where compression axis $\langle 1\,1\,0\rangle$ fiber develops high intensities.

The preform shape identified at various iterations of the design problem and the objective function over seven iterations are shown in Fig. 9. The optimal solution for the design problem is attained in the sixth iteration. The optimal preform shape corresponds to Bézier coefficients $\boldsymbol{\beta} = \{1.00639, 1.02940, 1.08443, 1.15127, 1.16593, 1.13392\}$. The preform shape at the final time step of the optimization problem for the first, second and final iteration of the design problem is shown in Fig. 10. The yield strength distribution on the curved surface at the end of forging at the first, second and final iteration are shown in

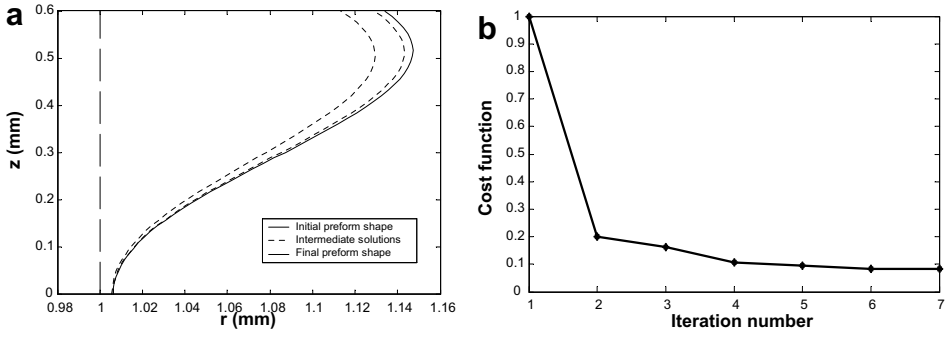

Fig. 9. (a) Profile of the curved surface of the preform at the initial, intermediate and final iterations of the design problem (b) decrease in cost function at successive iterations.

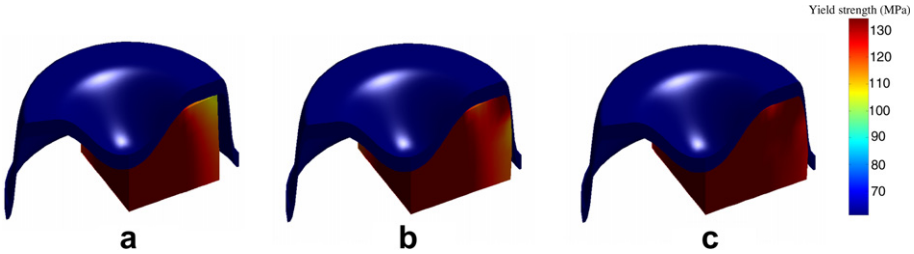

Fig. 10. Final configuration at the end of forging in the (a) first iteration (b) second iteration (c) final iteration.

Fig. 11. In the first iteration (Fig. 10a), the preform does not completely fill the die upon forging. Almost complete fill is obtained in as early as the second iteration (Fig. 10b) showcasing the efficiency of the design algorithm. However, in this iteration, the requirement of uniform yield strength is not met and as much as 30 MPa variation is seen on the curved surface in Fig. 11b. In the converged solution shown in Fig. 11c, both requirements are met and the variation in yield strength reduces to about 3 MPa on the curved surface.

4.3. Example 3. Design of yield strength distribution in complex forging operations using remeshing schemes

Complex metal forming simulations often lead to severe distortions in the initial mesh. As a result, periodic remeshing operations need to be carried out to ensure good element quality throughout the simulation. In the next two examples, an automatic remeshing capability is implemented. Once remeshing is complete, all history-dependent variables including deformed ODF grids at each integration point of the macro-scale, and the quantities s^{α}, $\overline{\boldsymbol{T}}$, $\boldsymbol{\omega}$, $\boldsymbol{F}^{e}$ and $\boldsymbol{F}^{p}$ at every integration point of the corresponding ODF are updated. The sensitivity counterparts of these quantities are also transferred in the same manner. In this problem, the forging of a FCC copper spheroidal preform to form a cross-shaft is considered. The primary objective is to design the preform for a final forged product (with fixed stroke) such that required shape is obtained. The secondary objective is the same as the previous problem, i.e. to minimize the variation of strength on the curved surface

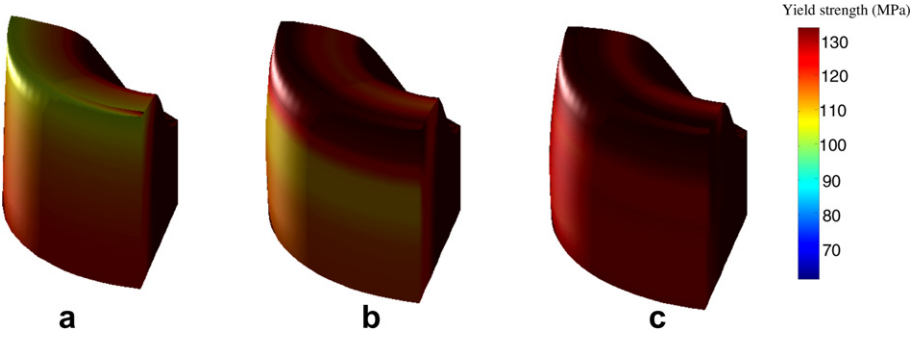

Fig. 11. Yield strength distribution on the curved surface at the end of forging at the (a) first iteration (b) second iteration (c) final iteration.

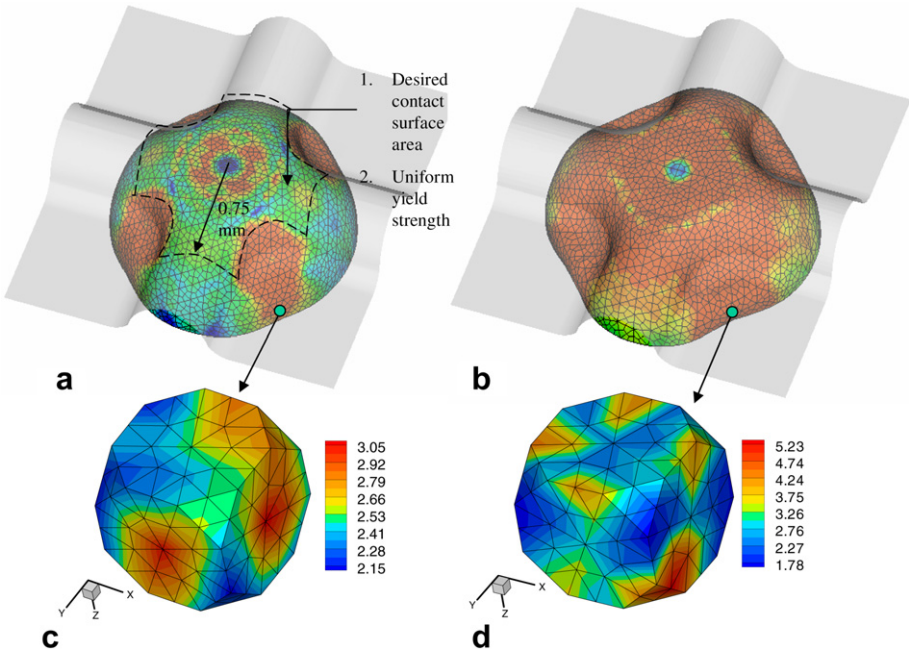

Fig. 12. Texturing at a representative material point during an (a) intermediate and (b) final time step of the closed-die forging problem. The objective function is described in (a).

of the final product. The objective function for the design problem is same as in the previous example. However, the objective function is only computed with a radius of 0.75 mm which is the required dimension of the cross-shaft as indicated in Fig. 12a.

For the design problem the free surface of the sphere is discretized using Bézier curves in a similar fashion as the previous example leading to a total of six design variables. The forging velocity was assumed to be 0.01 mm/s while the stroke was fixed at 0.1 mm. The shape parameters in the initial preform are $\beta_i = 0.7$ for all i. This corresponds to a spherical preform of radius 0.7 mm. The objective is to design the free surface (represented by the degree 6 Bézier curve) of the preform of fixed height $H = 0.70$ mm that when forged using the closed forming die results in the desired dimensions (contact radius of 0.75 mm) and uniform distribution of yield strength on the external surface after a specified stroke of 0.1 mm.

Fig. 12 shows an intermediate step (at 0.05 mm stroke) and the final forged product (at 0.1 mm stroke) at the optimal preform shape along with a representative ODF calculated at the material point marked in the figure. At the final time step the ODF (Fig. 12d) indicates a predominantly z-axis compression mode with the depletion of intensities from the z-axis $\langle 1\,0\,0\rangle$ fiber and development of strong z-axis $\langle 1\,1\,0\rangle$ fibers on the x- and y-face of the ODF. The preform shape identified at various iterations of the design problem and the objective function are shown in Fig. 13. The optimal preform shape corresponds to Bézier coefficients $\boldsymbol{\beta} = \{0.851, 0.847, 0.830, 0.810, 0.810, 0.755\}$. The preform shape and yield strength distribution at the final time step of the optimization problem for the first, second and final iteration of the design problem is shown in Fig. 14. The figure clearly shows the decrease in variability of yield strength in successive design iterations.

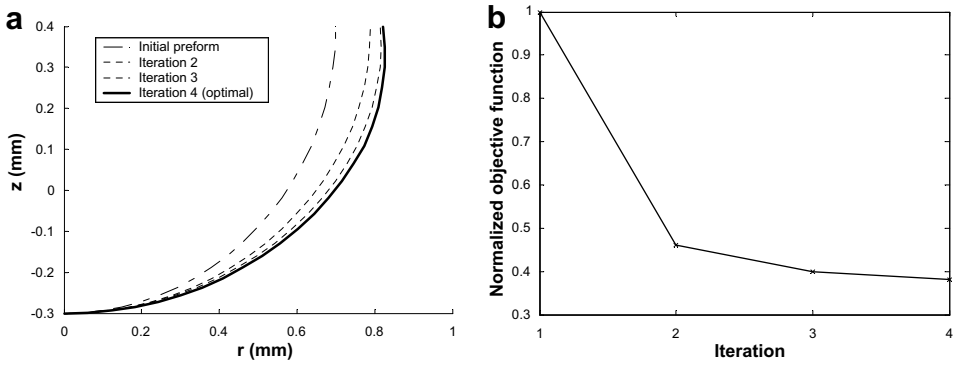

Fig. 13. (a) Profile of the curved surface of the preform at the initial, intermediate and final iterations of the design problem (b) Decrease in cost function at successive iterations.

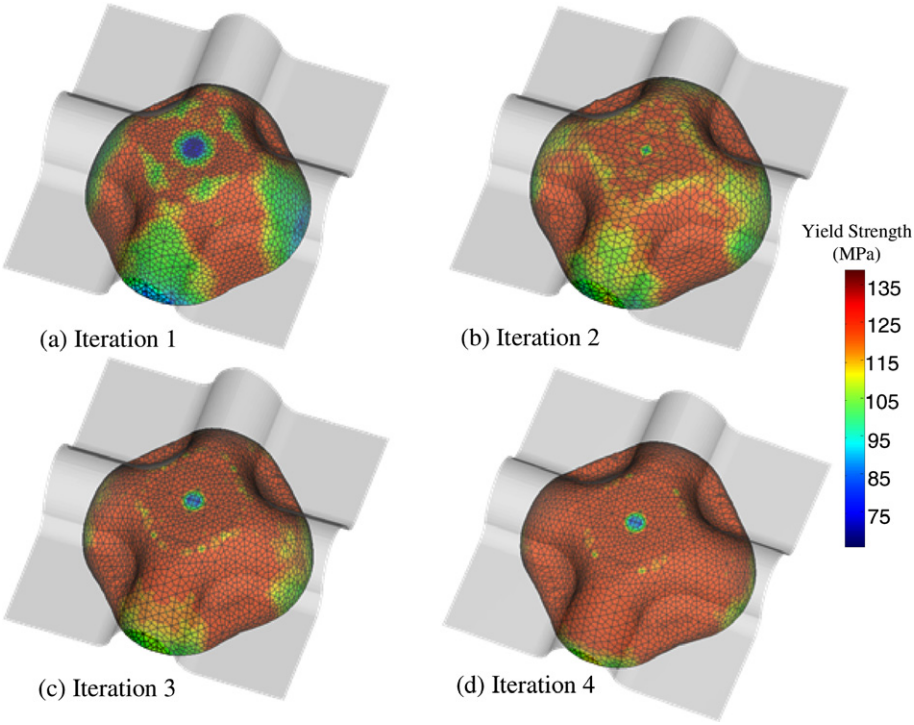

Fig. 14. Final configuration at the end of forging for various iterations of the design problem.

4.4. Example 4. Design of magnetic hysteresis losses in closed die forged components

When a ferromagnetic material is taken through a cycle of magnetization and demagnetization in an alternating current field, energy is spent in aligning the magnetization vectors of the individual crystals along the direction of the external applied field. This

alternating magnetization and demagnetization leads to a power loss in the material defined as hysteresis loss. Power losses also occur due to eddy currents. The total power loss can be expressed as a function of the external magnetization direction $\boldsymbol{h}$ by the expression (Hutchinson and Swift, 1972):

$$P(\boldsymbol{h}) = A_0 + A_1(l^2m^2 + m^2n^2 + l^2n^2) + A_2 l^2m^2n^2, \tag{38}$$

where P is expressed in W/kg and l, m and n are the direction cosines of $\boldsymbol{h}$ as represented in the crystal coordinate frame.

The coefficients A_0 and A_1 are different for the total power loss and the hysteresis loss and also depend on the frequency of magnetization. The coefficient A_2 is small and is generally ignored. FCC nickel is used as the deforming material with constitutive model parameters $h_o = 283$ MPa, $s_s = 240$ MPa, $a = 3.0$, $s_o = 16$ MPa calibrated using experimental results of Narutani and Takamura (1991). Elastic parameters of Nickel used are $C_{11} = 247$ GPa,$C_{12} = 147$ GPa and $C_{44} = 125$ GPa. For computation of magnetic hysteresis loss, the values $A_0 = 0$ and $A_1 = 10.0$ W/kg are used for computing the hysteresis loss of nickel at a frequency of 30 Hz (Acharjee and Zabaras, 2003). The corresponding polycrystal quantities can then be obtained by averaging over the ODF as in Eq. (2). The external magnetization direction in the sample coordinate system is taken as $(1/\sqrt{2}, 1/\sqrt{2}, 0)$.

The particular process involved is a closed-die forging of a circular disc. The primary objective is to design the preform for a final forged product such that the die cavity is fully-filled with minimal flash after a stroke of 4.8 mm. The secondary objective in this problem is to minimize the hysteresis loss on the curved surface (along the perimeter) of the final product. The objective function for the design problem is thus defined as

$$\min_{\boldsymbol{\beta}} \boldsymbol{F}(\boldsymbol{\beta}) = \frac{1}{N}\sum_{i=1}^{N}((\langle P\rangle_i(\boldsymbol{\beta}))^2) + \sum_{i=1}^{N^*}((r_i(\boldsymbol{\beta}) - r_i^{\text{desired}})^2 + (z_i(\boldsymbol{\beta}) - z_i^{\text{desired}})^2). \tag{39}$$

This example presents a forging process design for producing an axi-symmetric ribbed disk. The initial billet is a right cylinder of 0.6 mm height and 1.15 mm radius. The forging velocity is taken as 0.01 mm/s. The geometry of the finishing die is taken from Example 5.3 of Zabaras et al. (2003).

This example involves four remeshing operations at times 10, 20, 30 and 40 s. The ODF grids are also transferred to integration points of the new mesh through smoothing and data transfer operations. The details of the remeshing and data transfer procedure are the same as Example 3. The Bézier curve representation of the preform is given by Eq. (35). Fig. 15 shows an intermediate steps (at 0.22 mm and 0.44 mm stroke) of the preform shape in the second iteration along with a representative ODF calculated at the material point marked in the figure. At 0.22 mm stroke, the ODF shown closely represents ODFs obtained from plane strain compression along y-direction in the z–y plane. The texture is predominated by the α fiber connecting the ideal Goss and brass orientations on the x-face of the ODF. At 0.44 mm stroke, the z-axis tension texture becomes predominant due to compressive strains developing along both x- and y-direction as the preform progressively comes into contact with the die. This is evidenced by the loss of intensity in the z-axis $\langle 1\,1\,0\rangle$ fibers seen on the x- and y-faces of the ODF in Fig. 15d. The $\langle 1\,1\,0\rangle$ pole figures at 0.22 mm stroke and 0.44 mm stroke, respectively, as shown in Fig. 15c and e, show the progressive loss of intensities of the z-axis $\langle 1\,1\,0\rangle$ fibers due to the change in the predominant deformation mode from y-axis plane strain compression to z-axis tension.

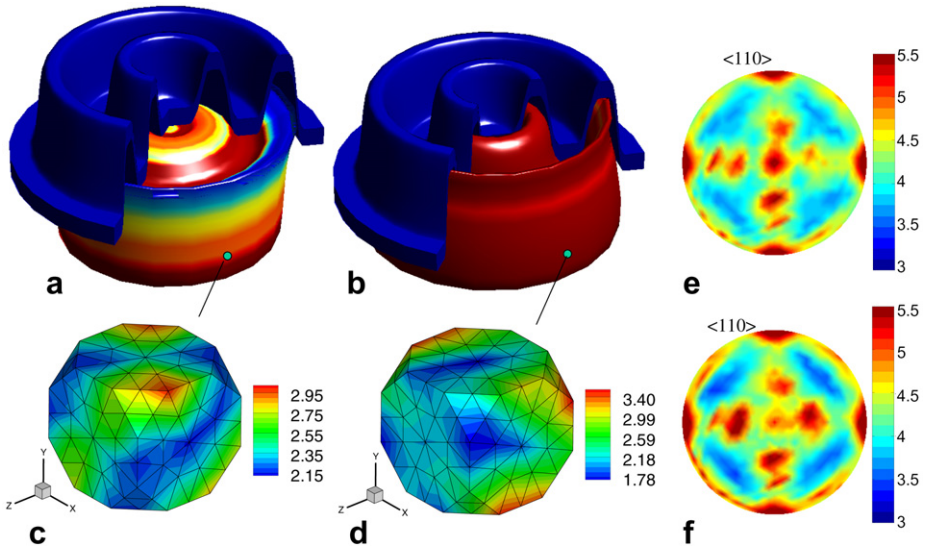

Fig. 15. (a, b) Yield strength distribution at 0.22 mm and 0.44 mm stroke (c, d) ODF at a point close to the bottom perimeter of the preform at 0.22 and 0.44 mm stroke. (e, f) The $\langle 1\,1\,0\rangle$ pole figures of the ODF at 0.22 and 0.44 mm stroke respectively.

Advantages are derived from the symmetry of Rodrigues' space relative to the sample axes. The effect of a permutation of the sample axes on texture results in a corresponding permutation of the axes of Rodrigues space without any alteration of the structure of the texture. For example, textures developed under compression along the y-axis as seen in Fig. 8d were associated with increase in intensities along y-axis $\langle 1\,1\,0\rangle$ fibers located on the z- and x-faces of the ODF. In the case of z-axis tension texture in Fig. 15d, decrease in intensities are found (by corresponding permutation of axis) along z-axis $\langle 1\,1\,0\rangle$ fibers located on the x- and y-faces of the ODF. In contrast, over the Euler angle space, permutations of sample axes modify the texture in complex ways.

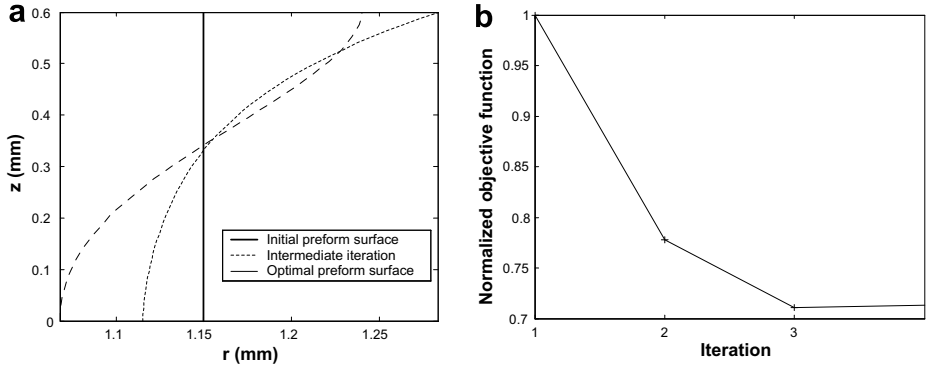

Fig. 16. (a) Profile of the curved surface of the preform at the initial, intermediate and final iterations of the design problem. (b) Decrease in cost function at successive iterations.

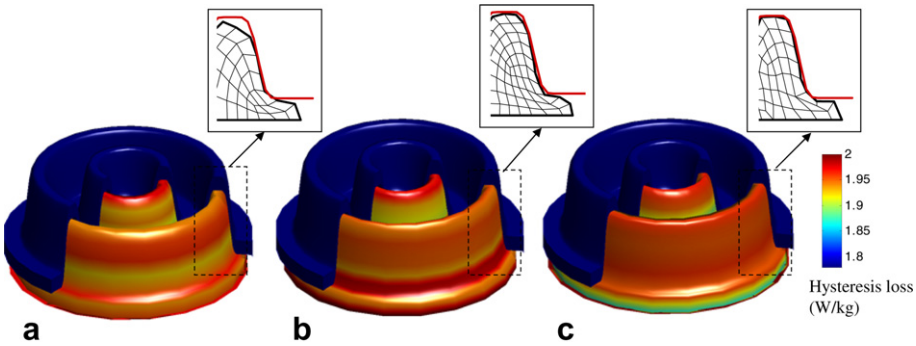

Fig. 17. Hysteresis loss distribution and the die cavity fill is illustrated in the (a) first iteration (b) second iteration (c) final iteration.

The optimal solution for the design problem is attained in four iterations. The preform shape identified at various iterations of the design problem and the objective function over four iterations are shown in Fig. 16. The optimal preform shape corresponds to Bézier coefficients $\boldsymbol{\beta} = \{1.0681, 1.0825, 1.1141, 1.1845, 1.2374, 1.2403\}$. The magnetic hysteresis loss distribution on the curved surface at the end of forging at the first, second and final iteration are shown in Fig. 17a–c respectively. In the first iteration, less material was used leading to large underfill. In the second iteration, the underfill reduces drastically, however, the magnetic hysteresis losses have not yet reached the optimal value. The final iteration gives the optimal decrease in magnetic hysteresis loss as well as allows complete filling of the die cavity as indicated in Fig. 17c.

5. Conclusions

Selection of macro-scale process parameters such as die shape, preform shape and forging velocity to control properties such as strength and stiffness is a challenging multi-scale problem due to the need to relate such macro-scale parameters with microstructure evolution. In this work, we presented a multi-scale optimization strategy for designing thermo-mechanical processes so that desired microstructure-sensitive properties are realized. Specifically, a two-scale continuum sensitivity formulation was developed that allows efficient computation of sensitivities of microstructure field variables such as slip resistances and texture with respect to perturbations in macro-scale forming parameters such as forging rates, die shapes and preform shapes. These sensitivities have been successfully employed in a gradient optimization framework for controlling properties such as hysteresis losses, the yield stress distribution and Young's modulus in complex deformation processes by optimally altering die and preform shapes.

The algorithm is computationally efficient and converges to the desired response within a few iterations. The simulator can also be easily extended towards computational design of other orientation-dependent properties such as thermal conductivity or the thermal expansion coefficient (Kocks et al., 2000) as well as in the design of devices with desired optical properties (Bunge, 1983). Other areas of applicability of this approach include calibration of material models or contact parameters through minimization of error between known experimental measurements and those predicted by the multi-scale model. The

extension of the technique to address materials design in multiple stage forming processes is needed but the modifications involved are rather straightforward (Zabaras et al., 2003). Effort is currently on to improve the micro-scale model by incorporating higher-order features such as grain size and orientation correlations, in addition to crystallographic texture, using finite element homogenization schemes (Sundararaghavan and Zabaras, 2006).

Acknowledgement

The work presented here was funded with grants to Cornell University by the Mechanical Behavior of Materials program (Dr. D. Stepp, program manager) of the Army Research Office (Grant W911NF-04-1-0283) and by the Computational Mathematics program (Dr. F. Fahroo, program manager) of the Air Force Office of Scientific Research (grant FA9550-04-1-0070). The large scale simulations reported here were performed at the MPDC laboratory's Linux cluster (available through AFOSR-DURIP funding) and at the Cornell Center for Advanced Computing.

References

Acharjee, S., Zabaras, N., 2003. A proper orthogonal decomposition approach to microstructure model reduction in Rodrigues space with applications to the control of material properties. Acta Materialia (51/18), 5627–5646.

Acharjee, S., Zabaras, N., 2006. The continuum sensitivity method for the computational design of three-dimensional deformation processes. Computer Methods in Applied Mechanics and Engineering 195, 6822–6842.

Adams, B.L., Henrie, A., Henrie, B., Lyon, M., Kalidindi, S.R., Garmestani, H., 2001. Microstructure sensitive design of a compliant beam. Journal of the Mechanics and Physics of Solids 49, 1639–1663.

Anand, L., Kothari, M., 1996. A computational procedure for rate-independent crystal plasticity. Journal of the Mechanics and Physics of Solids 44 (4), 525–558.

Asaro, R.J., 1983. Micromechanics of Crystals and Polycrystals. Advances in Applied Mechanics 23, 1–115.

Asaro, R.J., Needleman, A., 1985. Texture development and strain hardening in rate dependent polycrystals. Acta Metallurgica 33, 923–953.

Badrinarayanan, S., Zabaras, N., 1996. A sensitivity analysis for the optimal design of metal forming processes. Computer Methods in Applied Mechanics and Engineering 129, 319–348.

Balay, S., Buschelman, K., Eijkhout, V., Gropp, W.D., Kaushik, D., Knepley, M.G., McInnes, L.C., Smith, B.F., Zhang, H., 2004. PETSc Users Manual ANL-95/11 – Revision 2.1.5, Argonne National Laboratory.

Bronkhorst, C.A., Kalidindi, S.R., Anand, L., 1992. Polycrystalline plasticity and the evolution of crystallographic texture in FCC metals. Philosophical Transactions of the Royal Society of London A 341, 443–477.

Bunge, H.J., 1983. Texture Analysis in Materials Science. Butterworths.

Chenot, J.L., Massoni, E., Fourment, L., 1996. Inverse problems in finite element simulation of metal forming processes. Engineering Computations 13, 190–225.

Cuitiño, A.M., Ortiz, M., 1992. Computational modeling of single crystals. Modelling and Simulation in Material Science and Engineering 1, 225–263.

Ganapathysubramanian, S., Zabaras, N., 2002. A continuum sensitivity method for finite thermo-inelastic deformations with applications to the design of hot forming processes. International Journal for Numerical Methods in Engineering 55, 1391–1437.

Ganapathysubramanian, S., Zabaras, N., 2005. Modeling the thermoelastic–viscoplastic response of polycrystals using a continuum representation over the orientation space. International Journal of Plasticity (21/1), 119–144.

Hill, R., 1965. Continuum micro-mechanics of elastoplastic polycrystals. Journal of Mechanics and Physics of Solids 13, 89–101.

Hosford, W.F., 1993. The Mechanics of Crystals and Textured Polycrystals. Oxford University Press, New York.

Hutchinson, W.B., Swift, J.G., 1972. Anisotropy in some soft magnetic materials. Texture 1, 117–123.

Kalidindi, S.R., Houskamp, J.R., Lyons, M., Adams, B.L., 2004. Microstructure sensitive design of an orthotropic plate subjected to tensile load. International Journal of Plasticity 20 (8–9), 1561–1575.

Kocks, U.F., Tomé, C.N., Wenk, H.R., 2000. Texture and Anisotropy – Preferred Orientations in Polycrystals and their Effect on Materials Properties. Cambridge University Press, Cambridge.

Kumar, A., Dawson, P.R., 1996. The simulation of texture evolution with finite elements over orientation space I & II. Computer Methods in Applied Mechanics and Engineering 130, 227–261.

Kumar, A., Dawson, P.R., 1997. Modeling crystallographic texture evolution with finite elements over neo-Eulerian orientation spaces. Computer Methods in Applied Mechanics and Engineering 153, 259–302.

Lakes, R., 2000. Deformations in extreme matter. Science 288 (5473), 1976–1977.

Li, D.S., Garmestani, H., Adams, B.L., 2005. A texture evolution model in cubic–orthotropic polycrystalline system. International Journal of Plasticity 21 (8), 1591–1617.

Mandel, J., 1965. Generalization de la theorie de la plasticite de W.T. Koiter. International Journal for Solids and Structures 1, 273–295.

Mandel, J., 1972. Plasticite Classique et Viscoplasticite. CISM Courses and Lectures, vol. 97. Springer, Berlin.

Narutani, T., Takamura, J., 1991. Grain size strengthening in terms of dislocation density measured by resistivity. Acta Metallurgica et Materialia 39 (8), 2037–2049.

Olson, G.B., 1997. Computational design of hierarchically structured materials. Science 277 (5330), 1237–1242.

Rashid, M.M., Nemat-Nasser, S., 1990. Modeling very large plastic flows at very large strain rates for large scale computation. Computers and Structures 37, 119–132.

Rice, J.R., 1971. Inelastic constitutive relations for solids: an internal variable theory and its application to metal plasticity. Journal of Mechanics and Physics of Solids 19, 433–455.

Rollett, A.D., Storch, M.L., Hilsinki, E.J., Goodman, S.R., 2001. Approach to saturation in textured soft magnetic materials. Metallurgical and Materials Transactions A 32, 2595–2603.

Sigmund, O., Torquato, S., 1996. Composites with extremal thermal expansion coefficients. Applied Physics Letters 69, 3203–3205.

Sousa, L.C., Castro, C.F., Antonio, C.A.C., Santos, A.D., 2002. Inverse methods in design of industrial forging processes. Journal of Materials Processing Technology 128, 266–273.

Srikanth, A., Zabaras, N., 2000. Shape optimization and perform design in metal forming processes. Computer Methods in Applied Mechanics and Engineering 190, 1859–1901.

Srikanth, A., Zabaras, N., 2001. An updated Lagrangian finite element sensitivity analysis of large deformations using quadrilateral elements. International Journal for Numerical Methods in Engineering 52, 1131–1163.

Sundararaghavan, V., 2007. Multi-scale Computational Techniques for Design of Polycrystalline Materials, Ph.D. Dissertation, Sibley School of Mechanical and Aerospace Engineering, Cornell University, August 2007.

Sundararaghavan, V., Zabaras, N., 2006. Design of microstructure-sensitive properties in elasto-viscoplastic polycrystals using multi-scale homogenization. International Journal of Plasticity 22, 1799–1824.

Sundararaghavan, V., Zabaras, N., 2007. Linear analysis of texture-property relationships using process-based representations of Rodrigues space. Acta Materialia 55 (5), 1573–1587.

Taylor, G., 1938. Plastic strain in metals. Journal of the Institute for Metals 62, 307–324.

Teodosiu, C., Sidoroff, F., 1976. A theory of finite elastoviscoplasticity of single crystals. International Journal of Engineering Sciences 14, 165–176.

Zabaras, N., Ganapathysubramanian, S., Li, Q., 2003. A continuum sensitivity method for the design of multi-stage metal forming processes. International Journal of Mechanical Sciences 45, 325–358.

Zhao, G., Wright, E., Grandhi, R.V., 1997. Preform die shape design in metal forming using an optimization method. International Journal of Numerical Methods in Engineering 40, 1213–1230.